Earth Sciences
2023; 2(6): 188-197
http://www.sciencepublishinggroup.com/j/earth
doi: 10.11648/j.earth.20231206.11
ISSN: 2328-5974 (Print); ISSN: 2328-5982 (Online)

Research and Application of Different Coal Wall Spalling Forms

Yajun Xu[1, 2, *], Yibo Du[1, 2], Kun Zhang[3], Xiaoliang Pang[1, 2], Yongxiang Xu[1, 2]

[1]Coal Mining Research Branch, China Coal Research Institute, Beijing, China

[2]Coal Mining Research Institute Co. Ltd of CCTEG, Beijing, China

[3]Shandong Provincial Key Laboratory of Robotics and Intelligent Technology, Shandong University of Science and Technology, Qingdao, China

Email address:

xuyajun@tdkcsj.com (Yajun Xu), duyibo@tdkcsj.com (Yibo Du), zhangkunliaoning@163.com (Kun Zhang), 18811155301@163.com (Xiaoliang Pang), xuyongxiang@tdkcsj.com (Yongxiang Xu)

[*]Corresponding author

To cite this article:

Yajun Xu, Yibo Du, Kun Zhang, Xiaoliang Pang, Yongxiang Xu. Research and Application of Different Coal Wall Spalling Forms. *Earth Sciences*. Vol. 12, No. 6, 2023, pp. 188-197. doi: 10.11648/j.earth.20231206.11

Received: September 21, 2023; **Accepted**: October 23, 2023; **Published**: November 9, 2023

Abstract: Coal wall spalling is a key technical problem for surrounding rock control in fully mechanized mining face. For many years, coal wall spalling has mainly been studied through laboratory experiments based on coal samples, and in recent years, numerical simulation software has been used for simulation analysis. Theoretical research is mainly based on a two-dimensional coal wall model. At present, the academic circle divides the coal wall spalling into two forms: shear and tensile spalling. However, the mechanism of coal wall spalling was not clear, and it is difficult to describe the causes of different spalling forms in different coal seam conditions. To solve the above problems, according to the characteristics of coal wall spalling, a three-dimensional simplified model of rib spalling is derived based on the plane spline stress balance condition. Based on this, fully considering the influence of overburden pressure, coal rock interface cohesion, and internal friction angle on shear stress and internal shear stress of coal, the stress balance equation of the coal wall spalling body based on a three-dimensional wedge model is established, and the calculation formula of coal wall slope fracture angle is derived combined with the shear failure characteristics of soft coal and tensile failure characteristics of hard coal. The formula of coal wall fracture angle integrates parameters such as coal seam depth, dynamic pressure coefficient, coal rock interface cohesion and internal friction angle, Poisson's ratio, coal cohesion, and internal friction angle. The shear failure of soft coal and the tensile failure of hard coal are characterized by a unified formula. The effects of coal seam depth, coal rock interface cohesion and internal friction angle, coal cohesion and internal friction angle, Poisson's ratio, and other parameters on coal wall fracture angle are studied. The mechanism of soft coal seam, medium hard coal seam, and hard coal seam rib spalling is analyzed, and the characteristics of shear sliding failure of soft coal seam, block failure of medium hard coal seam and plate slope of hard coal seam are well explained. Taking the fully mechanized face with large mining height in the hard coal seam of Jinjitan coal mine as an example, the fracture angle of the coal seam is calculated, and the characteristics of coal wall spalling like plate shape are well explained, which provides a practical theoretical analysis method for the final solution of this problem.

Keywords: Rib Spalling, Coal Wall Rupture Angle, Poisson's Ratio, Shear Failure, Tension Failure

1. Introduction

Coal wall spalling is a common mining problem in fully mechanized mining face. For a long time, which had been studied extensively by many scholars. Wang JH [1] studied the mechanism and prevention measures of coal wall spalling in extremely soft, thick coal seam and put forward the idea that water injection can improve the shear strength of the coal body and prevent coal wall caving in extremely soft coal seam to a certain extent. Fang XQ et al. [2] analyzed the characteristics of soft coal caving by using the simplified two-dimensional sliding model and gave the

prevention method of coal wall caving in fully mechanized top coal caving face in soft coal seam. Yuan Y et al. [3] established a three-dimensional "wedge" model, analyzed the relevant factors affecting the stability of the "wedge", and drew the conclusion that the coal wall of the "Three Soft" large mining height face is mainly in the form of "wedge" sliding. Wu YP et al. [4] agreed that the failure form of the coal wall was mainly shear slip failure, and the shape of the sidewall was mainly an irregular quadrangular pyramid. In order to determine the position of the coal wall slope, some scholars use the principle of compression bar stability to study the characteristics of coal wall slope. The literature [5, 6] first studied the stability of coal wall with large mining height by using the pressure bar principle, and obtained that the position where the coal wall is prone to caving is 0.65 times higher than the mining height from the floor. Subsequently, some scholars also began to use this method to study the characteristics of coal wall caving [7-9]. Literature [10, 11] studied the characteristics of coal wall caving in 8.5-meter fully mechanized mining face with a large mining height with the help of the principle of pressure bar stability, and drew the conclusion that the position of coal wall caving is mainly located in the upper part of the coal seam. It should be noted that there are certain preconditions to simplify the coal wall into compression bar. It is relatively suitable for hard coal seams with high compressive strength, but there are problems for weak coal seams. In reference [12], the author analyzed the influence of different constraint conditions and coal properties on the stability of compression bar and came to the conclusion that soft coal seam is prone to sliding instability and hard and medium-hard coal seam is prone to bending instability. With the transfer of China's coal mining center from the east to the west, due to the relatively hard coal quality in the west, more and more scholars began to study the characteristics of hard coal caving. Song ZQ et al. [13] studied the influence of mining height, mining depth and coal hardness on coal wall caving, and draw the conclusion that the influence of coal hardness on coal wall caving is the most significant. Wang JH et al. [14] considered that the coal wall of a hard coal seam is mainly in the form of tension shear and tension crack based on the results of uniaxial tensile and triaxial compressive tests of different coal samples. Zhang JH et al. [15] consider that there are two failure forms of coal wall: shear and tensile crack, and come to the conclusion that improving the cohesion of coal seam can effectively prevent coal wall spalling. Xu YX et al. [16] took Jinjitan hard coal seam as the research object, established the "π" mechanical model of coal wall stability, and put forward multi-dimensional prevention and control measures of coal wall stability. With the increase of coal seam hardness, in recent years, the phenomenon of plate-like sidewall has appeared in some mining areas in the West. Some scholars [17, 18] analyzed the failure characteristics of hard coal plate-like sidewall, and studied the cracking failure mechanism of coal wall. At the same time, some scholars began to study the mechanism of coal wall caving from the perspective of the interaction between hydraulic support and surrounding rock. Zhang YL et al. [19] studied the influence of the initial support force of hydraulic support on the stability of coal wall, and came to the conclusion that improving the initial support force is conducive to improving the stability of coal wall. Based on the field practice results, Wang GF et al. [20] believe that the split structure of extensible canopy and face plate is the best for the hydraulic powered support. Chang JC et al. [21] analyzed the influence of two different canopy structures, hinged front canopy and integral canopy, on coal wall caving, and draw a conclusion that the integral canopy structure is conducive to restraining coal wall caving. In recent years, some scholars have begun to study the mechanism of the coal wall. Xu YJ [22-23] emphatically analyzed the action mechanism of advance bearing pressure on coal wall caving and coal wall limit stability height of different coal seam. Wu XM et al. [24] studied the mining face slope mechanism of “three soft” coal seam based on FLAC software. Li ZJ et al. [25] analyzed the form of 8.8-meter super-high coal wall based on on-site observation data.

It was not difficult to find that, at present, the academic circles basically agree that there are two types of coal wall shear and pull fracture, but the mechanism of coal wall shear and pull fracture is still not very clear. It was not possible to theoretically explain the relationship between the properties of coal body and the failure mode of the coal wall. Therefore, the reasons for the formation of different rib spalling types in soft coal seam, medium hard coal seam and hard coal seam could not be clearly explained. It was difficult to describe the width and depth of the rib spalling quantitatively. Therefore, based on the general stress balance equation and considering the role and influence of Poisson's ratio on coal wall failure, this paper established the estimation formula of coal wall fracture angle, revealed the variation characteristics of coal wall fracture angle in different coal seams, and explained the coal wall caving characteristics of soft coal seam, medium hard coal seam and hard coal seam, which could provide a reference for the solution of similar problems.

2. Model of Rib Spalling

Real rib spalling of mining face was shown in Figure 1. According to the failure shape, the rib spalling could be simplified as symmetrical 3D model as shown in Figure 2, where I-I, II-II, and III-III, respectively represent different profiles of the simplified model of rib spalling. The sections perpendicular to the X, Y and Z axes of the rib spalling were described in Figures 3 to 5. Among them, σ is normal stress, and τ is shear stress. The gray area in Figure 3 represents the coal wall, the blue area represents the coal wall failure surface, and the blue-filled area represents the research object of this paper. In order to determine the failure shape of the coal wall, the boundary lines of each section were derived respectively.

Figure 1. *Photo of rib spalling.*

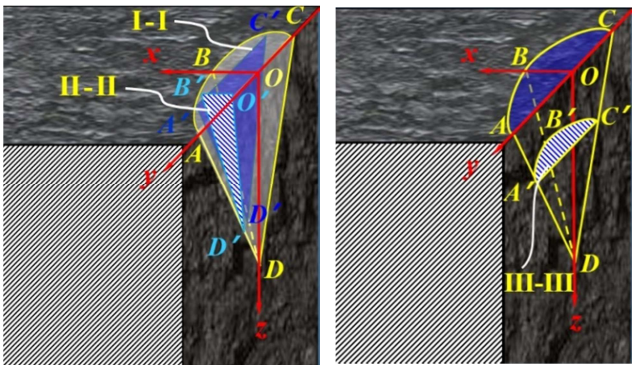

Figure 2. *Model of rib spalling*

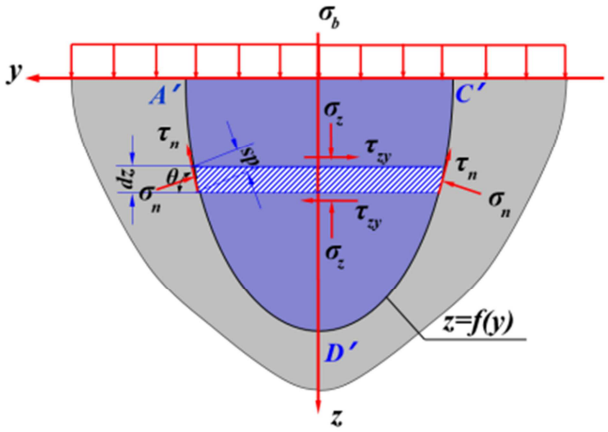

Figure 3. *Model of rib spalling yoz section(I-I).*

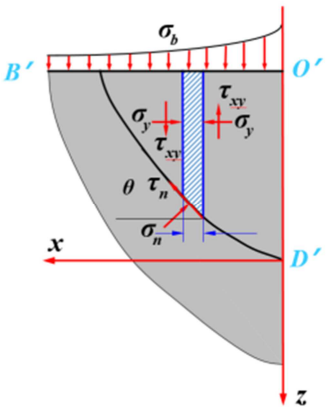

Figure 4. *Model of rib spalling xoz section (II-II).*

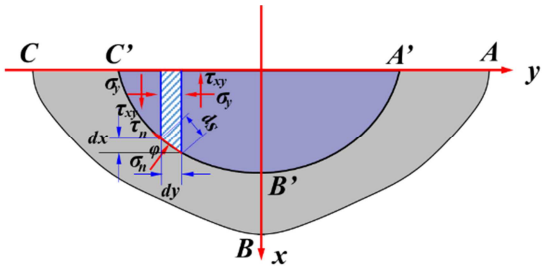

Figure 5. *Model of rib spalling xoy section(III-III).*

As shown in Figure 3, Any section parallel to the yoz plane was represented by $A'D'C'$. In particular, the section on the yoz plane is represented by ADC. According to the equilibrium conditions, taken the horizontal element as the research object, the vertical equation was shown below:

$$2\sigma_z \cos\theta ds = 2\tau_n \sin\theta ds + 2\sigma_n \cos\theta ds \tag{1}$$

If the rib spalling curve equation of the $A'D'C'$ plane was $z = f(y)$, the slope of the curve was $\tan\theta$. Assuming that the cohesion and friction angles of coal were C_0 and φ_0, the equation was derived from Mohr Coulomb law:

$$\frac{dz}{dy} = \frac{\sigma_z - \sigma_n}{C_0 + \sigma_n \tan\varphi_0} \tag{2}$$

According to the research from references [26, 27], the stress at the same distance from the coal wall along the mining face inclination direction in the range of a hydraulic support width changes very little and nearly constant. Therefore, σ_z and σ_n could be treated as constants. Where $K = \frac{\sigma_z - \sigma_n}{C_0 + \sigma_n \tan\varphi}$, K is constant. The rib spalling curve equation of the $A'D'C'$ plane could be described as $z = Ky + C$. The curve of rib spalling section parallel to the yoz plane approximated to a straight line.

As shown in Figure 4, Any section parallel to the xoz plane was represented by $B'O'D'$. According to the equilibrium conditions, taken the horizontal element as the research object, the vertical equation was shown below:

$$\sigma_b dx = \tau_n \sin\theta ds + \sigma_n \cos\theta ds + (\tau_{xz} + d\tau_{xz})dz \tag{3}$$

If the rib spalling curve equation of the $B'O'D'$ plane was $z = f(x)$, the slope of the curve was $z' = \tan\theta$. Based on the geometric features there were $dz = ds \cdot \sin\theta$ and $dx = ds\cos\theta$. Substitute this into eq. (3):

$$\sigma_b dx = \tau_n dz + \sigma_n dx + \tau_{xz} dz \tag{4}$$

Based on Mohr Coulomb law the eq. (5) could be deduced:

$$\frac{dz}{dx} = \frac{\sigma_b - \sigma_n}{\tau_n + \tau_{xz}} = \frac{\sigma_b - \sigma_n}{2C_0 + (\sigma_n + \sigma_z)\tan\varphi_0} \tag{5}$$

Because the vertical pressure distribution on coal wall is approximately exponential function distribution, the vertical pressure distribution could be described by eq. (6):

$$\sigma_b = Ke^{bx} + K_0 \tag{6}$$

In this equation $K_0 = -C_m \cot\varphi_m$, $b = \frac{\tan\varphi_m}{\lambda M}$, $K = (\gamma H + C_0 \cot\varphi_0)e^{\frac{\tan\varphi_0}{\lambda M}(M+L)}$. C_m and φ_m was the cohesion and friction angles of Coal-rock interface. Substitute eq. (6) into eq. (5):

$$\frac{dz}{dx} = K_c e^{bx} + K_1 \tag{7}$$

In this equation, $K_c = \frac{\gamma H + C_m \cot\varphi_m}{2C_0 + (\sigma_n + \sigma_z)\tan\varphi_0} e^{\frac{\tan\varphi_m}{\lambda M}(M+L)}$, $K_1 = -\frac{\sigma_n + C_m \cot\varphi_m}{2C_0 + (\sigma_0 + \sigma_z)\tan\varphi_0}$.

It could be known from eq. (7):

$$z = \frac{K_c e^{bx}}{b} + K_1 x + D \tag{8}$$

Expand e^{bx} by Taylor series. It was easy to take the first two terms of the expanded series. Substitute $e^{bx} = 1 + bx$ into eq. (8), the conclusion could be drawn that the longitudinal section curve of the rib spalling failure surface was approximately straight line.

As shown in Figure 5, taken $A'B'C'$ section of rib spalling body as research object. According to the equilibrium conditions, taken the vertical element as the research object, the equation was shown below:

$$\sigma_n \sin\varphi ds = \tau_n \cos\varphi ds \tag{9}$$

If the rib spalling curve equation of the $A'B'C'$ plane was $x = f(y)$, the slope of the curve was $\tan\theta$. Assuming that the cohesion and friction angles of coal were C_0 and φ_0, the equation was derived from Mohr Coulomb law:

$$y = (C_0/\sigma_n + \tan\varphi_0)x + C_2 \tag{10}$$

When σ_n was constant, $K_2 = \frac{C_0}{\sigma_n} + \tan\varphi_0$ could be constant. Which showed that the track line of the rib spalling transverse section was approximately straight.

In conclusion, the projections of rib spalling failure surfaces on xoy, xoz, and yoz planes were almost straight lines. The rib spalling could be described as wedges, as shown in Figure 6.

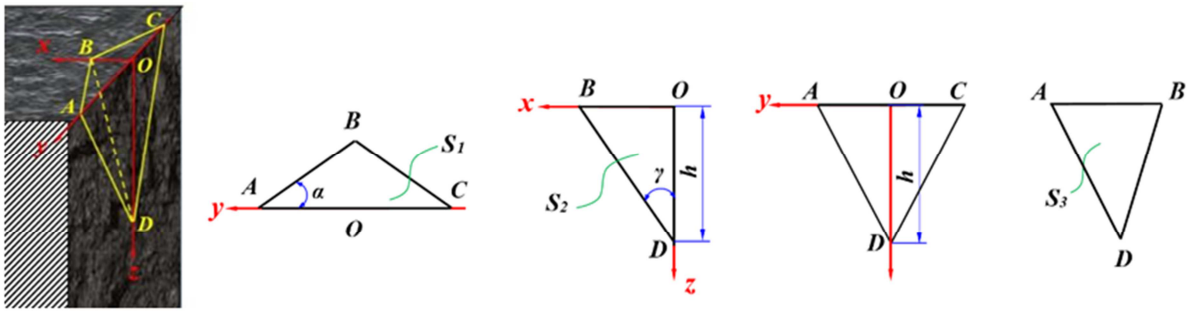

(a) (b) (c) (d) (e)

Figure 6. *Simplified model of rib spalling and its different sections.*

3. Stress Analysis of Rib Spalling Based on Wedge Model

The stress model of rib spalling could be shown in Figure 7a. The wedge block was divided into symmetrical triangular pyramid D-ABO and D-CBO, and the force analysis was carried out on them. Triangular pyramid D-ABO was subjected to normal stress σ_{z1}, shear stress τ_{z1} and the resultant force p on plane ABD. The plane ABD equation was $\frac{x}{\tan\gamma} + \frac{y}{\cot\alpha} + z - 1 = 0$, as shown in Figure 6, the projected areas of each surface were respectively $S_1 = h^2(\tan\gamma)^2 cot\alpha$, $S_2 = \frac{h^2 \tan\gamma}{2}$. In this equation h was height of rib spalling, γ was failure angle of coal wall. The normal vector was $\vec{n} = \{\cot\gamma, \tan\alpha, 1\}$ and the cosine of the normal vector $\vec{n}$ in the x, y, and z directions was:

$$\begin{cases} \cos\alpha_x = \dfrac{\cot\gamma}{\sqrt{1 + \tan^2\alpha + \cot^2\gamma}} \\ \cos\beta_y = \dfrac{\tan\alpha}{\sqrt{1 + \tan^2\alpha + \cot^2\gamma}} \\ \cos\gamma_z = \dfrac{1}{\sqrt{1 + \tan^2\alpha + \cot^2\gamma}} \end{cases} \tag{11}$$

In this equation, α_x, β_y, and γ_z was the angles between the normal vector $\vec{n}$ and the *x* axis, *y* axis, and *z* axis respectively. The component *forces* p_x p_y and p_z of the resultant force p along the x axis, y axis, and z axis were:

$$p_x = p\cos\alpha_x \quad p_y = p\cos\beta_y \quad p_z = p\cos\gamma_z \tag{12}$$

As shown in Figure 7a, according to the equilibrium conditions, taking the wedge model of rib spalling as the research object, the equation is shown below:

$$2p_x = \tau_z S_1, \quad 2p_z = \sigma_z S_1 \tag{13}$$

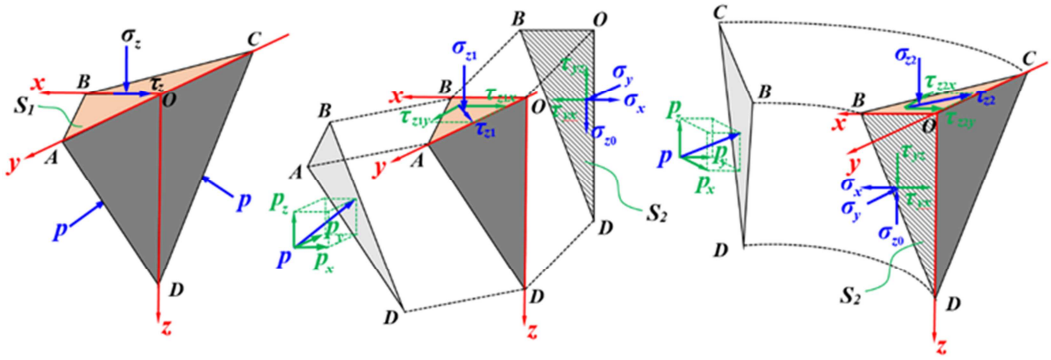

Figure 7. *Stress diagram of triangular pyramid rib spalling body.*

Taking the triangular pyramids D-ABO and D-CBO as the research objects (Figure 7a~Figure 7c), the equation is shown below:

$$p_x = \frac{\tau_{z1x}S_1}{2} - \sigma_x S_2 + \tau_{yx}S_2, \quad p_z = \frac{\sigma_{z1}}{2}S_1 + \sigma_{z0}S_2 - \tau_{yz}S_2 \tag{14}$$

$$p_x = \frac{\tau_{z2x}S_1}{2} + \sigma_x S_1 - \tau_{yx}S_2, \quad p_z = \frac{\sigma_{z2}}{2}S_1 - \sigma_{z0}S_2 + \tau_{yz}S_2 \tag{15}$$

The resultant force σ_z was composed of the normal stress σ_{z1} and σ_{z2} on the plane ABO and BCO. The resultant force τ_z was composed of the shear stress τ_{z1} and τ_{z2}. The resolution of shear stress τ_{z1} and τ_{z2} was τ_{z1x}, τ_{z1y}, τ_{z2x}, τ_{z2y}. Because triangular pyramid D-ABO and D-CBO were symmetrical structure, $\tau_{z1x} = \tau_{z2x}$. Juggle the eq. (13), (14) and (15), we could get the eq. (16):

$$p\cos\beta_y = \sigma_y S_2, \quad p\cos\alpha_x = \frac{\tau_z S_1}{2} \tag{16}$$

Substitute eq. (11) into eq. (16), the eq. (17) is shown below:

$$\begin{cases} \dfrac{p\tan\alpha}{\sqrt{1+\tan^2\alpha+\cot^2\gamma}} = \sigma_y S_2 \\ \dfrac{p\cot\gamma}{\sqrt{1+\tan^2\alpha+\cot^2\gamma}} = \dfrac{\tau_z S_1}{2} \end{cases} \tag{17}$$

Substitute S_1, S_2 into eq. (17) and divide the two equations in eq. (17):

$$(\tan\gamma)^2 = \frac{\sigma_y}{\tau_z} \tag{18}$$

Assuming that the cohesion and friction angles of Coal-rock interface were C_m and φ_m, so $\tau_z = C_m + \sigma_z\tan\varphi_m$. Substitute this into eq. (18), the Fracture angle of coal wall could be shown in eq. (19)

$$\gamma = a\tan\left(\sqrt{\frac{\sigma_y}{C_m + \sigma_z\tan\varphi_m}}\right) \tag{19}$$

Because the deformation of the coal wall in y direction was constrained, according to the research from references [28, 29],

$$\sigma_y = \mu(\sigma_x + \sigma_z) \tag{20}$$

3.1. Failure Characteristics of Soft Coal

Figure 7a and Figure 7b were physical photos of soft coal rib spalling. It could be seen from the figure that the coal wall of soft coal seam after rib spalling was very broken. The shape of rib spalling was generally the granular structure of powder (Figure 7a) or small block (Figure 7b) and accumulated in front of the conveyer. In addition, when the area of the rib spalling was large, it was difficult to see the obvious coal wall failure surface. As mentioned above, soft coal rib spalling was mainly shear failure [30, 31], which was characterized by large fracture angle and sufficient fracture of coal body, and obvious slip surface could be seen in small band (Figure 7c). This is because the cohesion of soft coal was small. Under the effect of pressure, the cohesion of coal body was destroyed first, and then the damaged material loused stability and slid under the effect of internal friction [32, 33]. As the coal body mainly expand to the side of the coal wall, when the horizontal strain exceeded the limit strain, we could get the eq. (21):

$$\sigma_x - \mu(\sigma_y + \sigma_z) = \sigma_c \tag{21}$$

Substitute eq. (21) into eq. (20), the eq. (22) was shown below:

$$\sigma_y = \frac{u\sigma_c}{1-u^2} + \frac{u\sigma_z}{1-u} \quad (22)$$

(a) [34] (b) [3] (c) [36]

Figure 8. *Photos of soft coal rib spalling.*

3.2. Failure Characteristics of Hard Coal

Figure 8a and Figure 8b were physical photos of hard coal rib spalling. It could be seen from the figure that the coal wall of soft coal seam after rib spalling was relatively intact and the shape of which was mainly block or plate type. Because hard coal has small Poisson ratio, large cohesive force and compressive strength, and small horizontal deformation. The failure form of hard coal was mainly tensile failure [37, 38] and the crack was mainly longitudinal (Figure 8c). As the longitudinal crack expands, the rib spalling began to be peeled off, and the peeling coal body was relatively complete, showing block or plate type. In essence, the failure was tensile strain fracture, that is, when the tensile strain reached the limit strain ε_3, the coal body was broken by tensile crack, and the failure condition was: $\sigma_x - \mu(\sigma_y + \sigma_z) = E\varepsilon_3$ [39]. If the compressive strength of coal body was σ_c, then $\sigma_c = E\varepsilon_c$. When $\varepsilon_3 = u_0\varepsilon_c$, then $\sigma_x - \mu(\sigma_y + \sigma_z) = u_0\sigma_c$. Substitute this into eq. (22), then:

$$\sigma_y = \frac{\mu_0 u\sigma_c}{1-u^2} + \frac{u\sigma_z}{1-u} \quad (23)$$

In this equation, u_0 was tension coefficient; $\sigma_c = \frac{2C_0\cos\varphi_0}{1-\sin\varphi_0}$ [40, 41], C_0 was cohesion and φ_0 was frictional angle.

Combined eq. (22) and Eq. (23) into one equation, and substituted $\sigma_z = K\gamma H$ into this equation, then:

$$\sigma_y = \frac{u_0 u\sigma_c}{1-u^2} + \frac{uK\gamma H}{1-u} \quad (24)$$

In this equation, K was dynamic pressure coefficient. When $u_0 = 1$ then shear failure was come up and when $u_0 > 1$ then tensile failure was come up. Substitute eq. (24) into eq. (19), the fracture angle of coal wall was as shown:

$$\gamma = a\tan\left(\sqrt{\frac{u_0 u\sigma_c + (u+u^2)K\gamma H}{(C_m + K\gamma H\tan\varphi_m)(1-u^2)}}\right) \quad (25)$$

The eq. (25) was the formula for calculating the fracture angle of the coal wall considering the shear stress of coal-rock interface and the shear stress of coal body.

(a) (b) (c) [42]

Figure 9. *Photos of hard coal wall spalling.*

4. Influence Factors of Coal Wall Fracture Angle

According to eq. (25), the coal wall fracture angle was affected by the buried depth of coal seam, coal-rock interface conditions, Poisson's ratio of coal body, cohesion of coal seam, internal friction angle and dynamic pressure coefficient. The influence of the above parameters on the coal wall fracture angle was analyzed below. The calculation parameters were as follows: the buried depth of coal seam is 240m, the dynamic pressure coefficient is 1, the bulk density of rock mass is 2.5t/m^3, and the bulk density of coal mass is 1.3t/m^3.

(1) Coal-rock interface conditions

The relevant parameters were as follows: Coal cohesion 1.5MPa, coal internal friction angle 35°, Poisson's ratio 0.2, coal-rock interface friction angle 35°. When the cohesion of coal-rock interface increased from 1MPa to 9MPa, the fracture angle trend of coal wall was shown in Figure 10a; If the cohesion of coal-rock interface was 3MPa and other parameters remained unchanged, when the internal friction angle of coal-rock interface increased from 10° to 50°, the fracture angle trend of coal wall was shown in Figure 10b. It could be seen from the figure that the fracture angle of coal wall decreased with the increase of cohesion and internal friction angle of coal-rock interface.

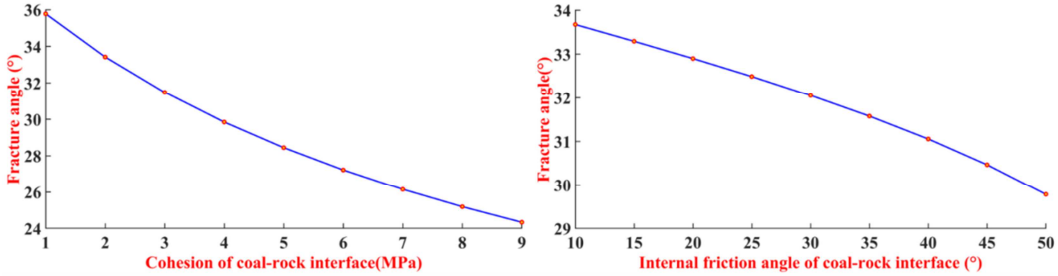

(a) (b)

Figure 10. *Influence of coal-rock interface conditions on fracture angle.*

(2) Coal body conditions

The relevant parameters were as follows: Poisson's ratio 0.2, coal internal friction angle 35°, Coal cohesion 3MPa, coal-rock interface friction angle 35°, the other parameters were the same as above. When coal cohesion increased from 1MPa to 9MPa, the coal wall fracture angle trend was shown in Figure 11a. The internal friction force of coal was 2.5MPa, and other parameters are the same as above. When the internal friction angle of coal increased from 10° to 50°, the fracture angle trend of coal wall was shown in Figure 11b. According to the figure, the coal wall fracture angle increased with the increase of coal body cohesion and internal friction angle.

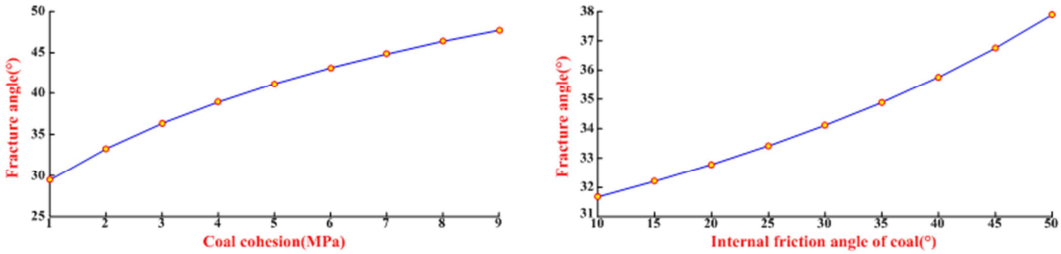

(a) (b)

Figure 11. *Influence of coal conditions on fracture angle.*

(3) Poisson's ratio and buried depth of coal seam

When the buried depth of coal seam increased from 300m to 900m, the coal wall fracture angle trend was shown in Figure 12a. According to the figure, the coal wall fracture angle decreased with the increase of buried depth. The cohesion of coal was 0.7MPa, the friction of coal was 38.5°, the cohesion of coal-rock interface was 2.8MPa, and the friction angle of coal-rock interface was 38°. Other parameters were the same as above. The relationship between Poisson's ratio of coal and the fracture angle of coal wall was shown in Figure 12b. According to the figure, when other conditions remained unchanged, the coal wall fracture angle increased with the increase of Poisson's ratio.

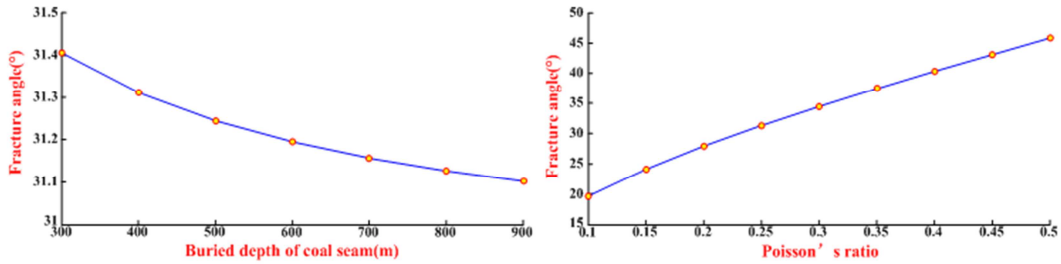

(a) (b)

Figure 12. *Influence of depth and Poisson's ratio on fracture angle.*

It could be seen from Figure 10 that the fracture angle of coal wall increased with the decrease of cohesion and internal friction of coal-rock interface. This is because when the cohesion and internal friction of the coal-rock interface were relatively small, in order to ensure the balance of the coal wall, the pressure affected deeper coal seam, and more areas of the coal-rock interface were affected. As a result, the failure depth of the coal wall increased, so the fracture angle increased.

According to Figures 10-12, Poisson's ratio had the most obvious influence on the coal wall fracture angle, while the buried depth had the weakest influence, relative to the coal-rock interface, coal body condition and buried depth. Because the overburden pressure was proportional to the buried depth, it indicated that the fracture angle of coal seam mainly depends on the properties of coal seam, especially the Poisson's ratio of coal body.

As shown in Figure 13a, if the height of the wall remained unchanged, the fracture angle of the coal wall decreased with the decrease of Poisson's ratio, and the shape of the failure surface of the coal wall transformed from parabolic to lamellar. This is due to the different Poisson's ratio between hard and soft coal seam. Under the same pressure, due to Poisson's ratio being higher, the transverse deformation of the coal wall free surface direction was large, and compressive strength of soft coal was low. When the cohesion of coal body was destroyed, the broken coal body mainly slid from the coal wall in the way of shear slip, which manifested as large collapse surface of the coal wall and broken rib spalling body. Hard coal seam Poisson's ratio was relatively small, while the coal seam transverse deformation was small and the compressive strength of hard coal was high. The coal wall had a certain compressive capacity. When the cohesion of the coal body was destroyed, longitudinal cracks occurred because of tensile failure in the coal wall. With the continuous expansion of the longitudinal cracks, the rib spalling occurred and the shape of which was block or plate sheet. We could draw the conclusion that due to the difference of Poisson's ratio, the lateral deformation of different coal seams under overburden pressure was different, which made different fracture angle for the coal wall, and then the shear failure or tension failure occurred and the rib spalling was block or plate shape and so on, in different forms. Therefore, Equation (17) could explain the different characteristics of the rib spalling as shown in Figure 13. The rib spalling in soft coal seam appeared parabolic (Figure 13b), which appeared block-like in middle and hard coal seam (Figure 13c) and plate-like in hard coal seam (Figure 13d).

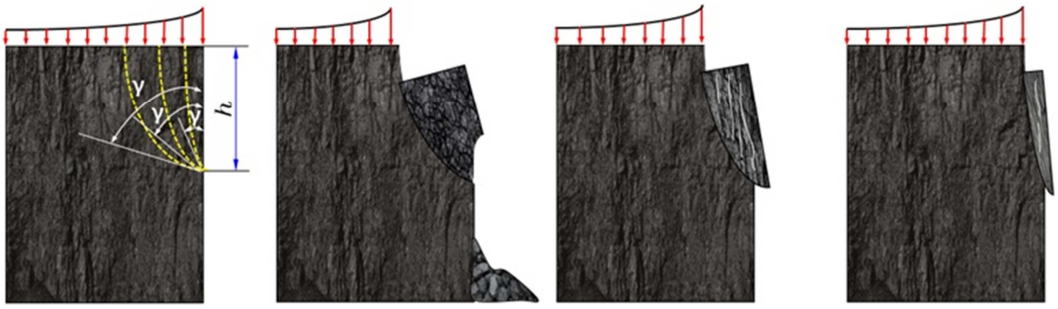

(a) (b) (c) (d)

Figure 13. *Schematic diagram of different rib spalling of coal wall.*

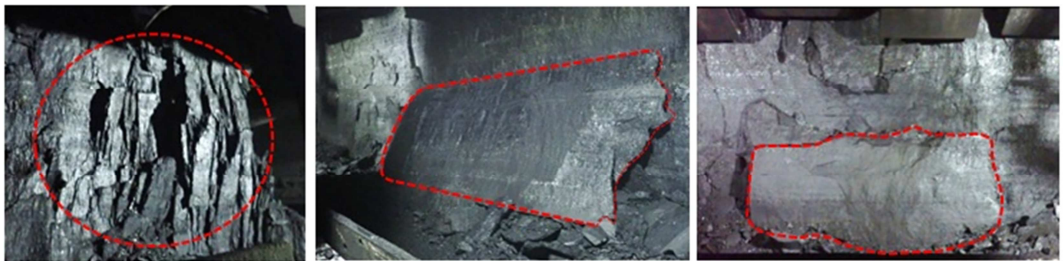

(a) (b) (c)

Figure 14. *Photos of coal wall spalling with plate form.*

5. Application Example

The mining face of Jinjitan Coal Mine form Yulin province, China, is about 300m deep; the thickness of coal seam is 7.99-12.49m; the internal friction angle of coal sample is 30.7°; and the cohesion is 2.1 MPa. ZY21000/38/82d hydraulic support was used in the fully mechanized mining with a large mining height. Due to the high hardness of coal seam, when the mining height was more than 7.5m, plate flaps shape of rib spalling, as shown in Figure 14, were often encountered [43]. If the dynamic pressure coefficient is 3, Poisson's ratio is 0.15, the cohesion of coal-rock interface and internal friction angle are 2.8 MPa and 42° respectively, the bulk density of rock mass is 2.5 t /m^3, and the bulk density of coal body is 1.3 t/m^3, the

calculation result of coal wall fracture angle is 25.5° based on eq. (25). The coal wall fracture angle is small, and the coal wall is mainly plate and slab. The theoretical results were basically consistent with the production practice.

6. Conclusion

(1) The change of coal wall fracture angle caused by soft coal shear failure and hard coal tensile failure could be characterized by a unified formula. By studying the variational characteristics of the coal wall fracture angle, the shear slip of soft coal seam, the block failure of medium and hard coal seam and the spalling of hard coal seam could be well explained.

(2) The coal wall fracture angle was affected by the buried depth of the coal seam, the coal-rock interface conditions, the properties of coal seam (Poisson's ratio, cohesion, internal friction angle) and the dynamic pressure coefficient. Poisson's ratio had the most significant effect on the coal wall fracture angle. The fracture angle of coal wall increased with the increase of Poisson's ratio, coal cohesion, and internal friction angle and decreased with the increase of buried depth, coal and rock interface cohesion, and internal friction.

(3) The soft coal seam with a large Poisson's ratio mainly experienced shear failure. The transverse deformation of the coal body was large, the depth of rib spalling was large, and the rib spalling body fell off in the way of shear slip. The hard coal seam with higher hardness was mainly damaged by tension, which caused it to crack longitudinally. With the expansion of the longitudinal crack, the rib spalling body was peeling off the coal wall in the form of block or plate.

References

[1] WANG JH. Mechanism of the rib spalling and the controlling in the very soft coal seam. Journal of China Coal Society, 2007, 32(8): 785-788.

[2] Fang XQ, He J, Li HC. A study of the rib mechanism in soft coal and its control at a fully-mechanized top-coal caving face [J]. Journal of China University of Mining & Technology, 2009, 38(5): 640-644.

[3] Yuan Y, Tu SH, MA XT, et al. Coal wall stability of fully mechanizing mining face with great mining height in "three-soft" coal seam and its control technology [J]. Journal of Mining & Safety Engineering, 2012, 29(1): 21-25.

[4] Wu YP, Lang D, Xie P. Mechanism of disaster due to rib spalling at fully-mechanized top coal caving face in soft steeply dipping seam [J]. Journal of China Coal Society, 2016, 41(8): 1878-1884.

[5] Yin XW, Yan SH, An Y. Characters of the rib spalling in fully mechanized caving face with great mining height [J]. Journal of Mining & Safety Engineering, 2008, 25(2): 222-225.

[6] Ning Y. Mechanism and control technique of the rib spalling in fully mechanized mining face with great mining height [J]. Journal of China Coal Society, 2009, 34(1): 50-52.

[7] Yang JX, Liu CY, Wu FF. The research on the coal wall stability mechanism in larger height coal seam with a stratum of gangue [J]. Journal of Mining & Safety Engineering, 2013, 30(6): 856-862.

[8] Huang QX, Liu JH. Vertical slice model for coal wall spalling of large mining height longwall face in shallow seam [J]. Journal of Mining & Safety Engineering, 2015, 32(2): 187-191.

[9] Zhang HW, Fu X, Shen YZ. Study on rib spalling mechanism and spalling depth in large mining height fully-mechanized face, in NajAziz and Bob Kininmonth [C]. Proceedings of the 2016 Coal Operators' Conference, Mining Engineering, University of Wollongong, 2019: 204-212.

[10] Wu H, Song XM. Theoretical analysis on coal wall stability of fully mechanized 8.5m high cutting longwall mining face [J]. Coal Science and Technology, 2015, 43(3): 22-25.

[11] Di S, Wang JR, Song GJ. Study on rib spalling characteristics of 8.5m height fully mechanized mining face. Coal Science and Technology, 2017, 45(9): 97-102.

[12] Xu YJ. Coal wall spalling mechanism studying and it's prevention method [J]. Coal Mining Technology, 2017, 22(1): 41-46.

[13] Song ZQ, Liang SK, Tang JQ, et al. Study on the influencing factors of coal wall rib spalling in fully mechanized working face [J]: Journal of Hunan University of Science & Technology (Natural Science Edition): 2011, 26(1): 1~4.

[14] Wang JH, Wang ZH, Kong DZ. Failure and prevention mechanism of coal wall in hard coal seam [J]. Journal of China Coal Society, 2015, 40(10): 2243-2250.

[15] Zhang JH, Li MZ, Yang ZK, et al. Mechanism of coal wall spalling in super high fully mechanized face and its multi-dimensional protection measures [J]. Journal of Mining & Safety Engineering, 2021, 38(3): 487-495.

[16] XU YX, Wang GF, Li MZ, et al. Investigation on coal face slabbed spalling features and reasonable control at the longwall face with super large height and longwall top coal caving method [J]. Journal of China Coal Society, 2021, 36(5): 728.

[17] XU YX, Wang GF, Li MZ, et al. Mechanism of slabbed spalling failure of the coal face in fully mechanized caving face with super large cutting height [J]. Journal of Mining & Safety Engineering, 2021, 38(1): 19-30.

[18] Yan JH. Analysis on interaction relationship between initial support load of powered support and surrounding rock in fully-mechanized coal mining face [J]. Coal Science and Technology, 2014, 42(4): 12-15.

[19] Zhang YL, Liu JF, Pang YH, et al. Effect analysis of prevention rib spalling system in hydraulic support [J]. Journal of China Coal Society: 2011, 36(4): 691-695.

[20] Wang GF, Pang YH, Liu JF. Determination and influence of cutting height of coal by top coal caving method with great mining height in extra thick coal seam [J]. Journal of China Coal Society: 2012, 37(11): 1777-1782.

[21] Chang JC, Xie GX, Zhang XH. Analysis of rib spalling mechanism of fully-mechanized top-coal caving face with great mining height in extra-thick coal seam [J]. Rock and Soil Mechanics, 2015, 36(3): 803-808.

[22] Xu YJ. Study on parameter optimization and coupling relation between surrounding rock and 2-leg powered support [D]. Coal Science Research Institute, 2013.

[23] Xu YJ. Research and application of coal wall limit stability height based on wedge model [J]. Chinese Journal of Rock Mechanics and Engineering, 2022, 41(Sup. 2): 3240-3248.

[24] Wu XM, Lei ZY, Wen J, et al. Experiment on prevention and control of coal wall spalling in three soft coal seam working face [J]. Coal Science and Technology, 2022, 50(9): 20-29.

[25] Li ZJ, Ji Z. Causes of rib spalling and the prevention measures in 8. 8m super-high mining face [J]. Coal Engineering, 2021, 53(11): 30-35.

[26] Xu YJ, WANG Guofa, ZHANG Jinhu, et al. Theory and application of supporting stress fields of hydraulic powered support groups in fully mechanized mining face with large mining height based on elastic supporting beam model [J]. Chinese Journal of Rock Mechanics and Engineering, 2018, 37(5): 1226-1236.

[27] Wang GF, Zhang JH, Xu YJ, et al. Supporting stress characteristics and zonal cooperative control technology of long mining face in deep thick coal seam [J]. Journal of China Coal Society, 2021, 46(3): 763-773.

[28] Qian MG. Mining pressure and strata control [M]. Coal Industry Press: Beijing, 1986: 48.

[29] Jiang FX, Liu JH, Wang P. Model of coal burst and instability based on Druker-Prager yield criterion [J]. Journal of China Coal Society, 2011, 36(5): 728.

[30] Sun Y, Li G, Zhang N, et al. Development of ensemble learning models to evaluate the strength of coal-grout materials [J]. International Journal of Mining Science and Technology, 2020, 31(2): 153-162.

[31] Wang JC, Wang ZH. Systematic principles of surrounding rock control in longwall mining within thick coal seams [J]. International Journal of Mining Science and Technology, 2019, 29(1): 64-70.

[32] Shen ZJ. Breakage mechanics and double-medium model for geological material [J]. Hydro-Science and Engineering, 2002, (4): 1-6.

[33] Shen ZJ, Liu EL, Chen TL. Generalized stress-strain relationship of binary medium model for geological materials [J]. Chinese Journal of Geotechnical Engineering, 2005, 27(5): 489-494.

[34] Liu S, Yang K, Tang CN. Mechanism and integrated control of "Rib Spalling: roof collapse-support instability" Hazard Chains in steeply dipping soft coal seams [J]. Advances in Materials Science and Engineering, 2021, 5: 4.

[35] J. Galvin. Coal burst on longwall B2 face at Austar coal mine on 19 August 2016 [A]. Mine safety, NSW Department of Industry: New South Wales, 2016: 6.

[36] John Cornwell. The Colliery photographs of John Cornwell. https://museum.wales/articles/ 1035/ The-Colliery-photographs-of-John-Cornwell.

[37] Li G, Li Z, Du F, et al. Study on the failure characteristics of coal wall spalling in thick coal seam with gangue [J]. Advances in Civil Engineering, 2020, (2): 1-10.

[38] Bai QS, Zhang XQ, Zhang C, et al. Numerical modelling on brittle failure of coal wall in longwall face-a case study [J]. Arabian Journal of Geosciences, 2014, 7(12): 5067-5080.

[39] Sun GZ, Sun Y. Principle of rock mechanics [J]. Science Press: Beijing, 2011: 71-76.

[40] An M, Yu MH, Wu X, et al. Generalized twin shear stress yield criterion in rock mechanics [J]. Rock and Soil Mechanics, 1991, 12(10): 17-26.

[41] Xie QD, He J, Liu J, et al. Unified twin shear strength theory for calculation of earth pressure [J]. 2003, 25(3): 344.

[42] Mark Colwell, Christopher Mark. Analysis and Design of Rib Support (ADRS) a rib support design mythology for Australian collieries [J]. Proceedings of the 24th International Conference on Ground Control in Mining. Morgantown, WV: West Virginia University, 2005: 12-22.

[43] Xu YX. Study on Structure Coupling between Hydraulic Roof Support and Surrounding Rock in Extra-thick and Hard Coal Seam with Super-large Mining Height and Longwall Top Coal Caving Method [D]. China Coal Research Institute, 2020.